Available online at www.sciencedirect.com
ScienceDirect
Journal of Photochemistry and Photobiology A: Chemistry 193 (2008) 271–283
Journal of Photochemistry and Photobiology A:Chemistry
www.elsevier.com/locate/jphotochem

Photocatalytic degradation of domoic acid using nanocrystalline TiO_2 thin films

Y. Djaoued [a,*], M. Thibodeau [a], J. Robichaud [a], S. Balaji [a], S. Priya [a], N. Tchoukanova [b], S.S. Bates [c]

[a] *Laboratoire de Micro-spectroscopies Raman et FTIR, Université de Moncton, Campus de Shippagan, 218 boul, J.-D. Gauthier, Shippagan, NB E8S 1P6, Canada*
[b] *Institut de Recherche sur les Zones cotières, Université de Moncton, Campus de Shippagan, 232-B, Avenue de l'église boul. J.-D. Gauthier, Shippagan, NB, E8S 1J2, Canada*
[c] *Fisheries and Oceans Canada, Gulf Fisheries Centre, P.O. Box 5030, Moncton, NB E1C 9B6, Canada*

Received 1 February 2007; received in revised form 6 July 2007; accepted 7 July 2007
Available online 12 July 2007

Abstract

Domoic acid (DA) is a water-soluble marine neurotoxin produced and released by *Pseudo-nitzschia* species. It is remarkably pervasive in North American coastal waters, where it is a threat to public health and some marine life, and has resulted in severe economic losses in the shellfish and crustacean harvesting industry. In this paper we report on the development of nanocrystalline titania thin films that were used as photocatalyst in the UV photodegradation of DA. TiO_2 thin films produced by a sol–gel dip-coating method in the presence of polyethylene glycol (PEG) of different molecular weights (200, 400 and 600), were deposited on glass and fused quartz substrates, and crystallized at different temperatures (90, 500 and 900 °C). The films were characterized using UV–vis, FTIR, SEM, XRD, and Raman spectroscopy. For the photocatalytic activity measurements, the TiO_2 films were immersed in a DA solution (2500 ng/mL) and exposed for various times at room temperature to UV irradiation ($\lambda \sim 350$ nm). DA analysis was carried out by HPLC, and the photocatalytic activity was quantified as the rate of disappearance of DA. The photocatalytic activity of the TiO_2 thin films was studied as a function of their crystallization temperature, type of PEG content, and thickness. The films prepared at low temperature proved to be very efficient photocatalysts. They showed a higher photocatalytic activity than those produced at high temperature. Also, using PEG of higher molecular weight in the TiO_2 coating solutions increased the effectiveness of the degradation. When using UV irradiation alone, without photocatalyst, the degradation of DA was not significant. The presence, transformation, and degradation of various DA isomers were observed during the photodegradation process, and a photodegradation mechanism is proposed.

Keywords: Domoic acid; Low temperature crystallization; Nanocrystalline TiO_2 thin film; Photocatalytic activity; Photodegradation mechanism

1. Introduction

Domoic acid (DA) is a water-soluble marine neurotoxin produced and released by certain species of the diatom genus *Pseudo-nitzschia* [1,2]. It is concentrated by filter-feeding animals and when consumed it causes gastrointestinal distress, dizziness, short-term memory loss and fatal brain damage. This syndrome is called amnesic shellfish poisoning (ASP). DA is remarkably pervasive in coastal waters of most continents worldwide, where it is a threat to public health and some marine life, and has resulted in severe economic losses in molluscan shellfish and crustacean harvesting industries. DA was originally discovered as the causal agent in an episode of fatal human poisoning in Prince Edward Island, in eastern Canada, in the autumn of 1987 [3]. At several other instances and locations in other parts of the world, DA has resulted in the mortality of hundreds of marine birds, mammals and fish [4,5]. Hence, considerable research has been focussed towards the detection, chemistry, and biological activity of DA. Degradation of DA has been a subject of study in marine and freshwater environments. Biodegradation of DA by a bacterium found in blue mussels was reported by Stewart et al. [6]. In order to understand the activity of DA released in water, Bates et al. [7] studied the photodegradation of DA in seawater and deionized water with the

* Corresponding author. Tel.: +1 506 336 3412; fax: +1 506 336 3434.
E-mail address: djaoued@umcs.ca (Y. Djaoued).

1010-6030/$ – see front matter © 2007 Elsevier B.V. All rights reserved.
doi:10.1016/j.jphotochem.2007.07.006

addition of iron as trace metal. They found that DA, which was present in the seawater along with Fe(III), degraded significantly under the irradiation of the full spectrum of light (UV–vis). This degradation was rapid in the first 5 h of radiation, and complete degradation occurred after 24 h. Recently, Fisher et al. [8] reported on the influence of Fe(III), phosphate and nitrate ions in the degradation of DA in the marine environment. They found that a significant amount of DA was degraded, with a half life of 14–15 h, in the presence of 3 μM Fe(III). They suggested that Fe(III) forms a complex with DA in a high pD (>5) and facilitates the photodegradation through a ligand–metal photoinduced charge transfer.

Marine biotoxins have a direct impact on the molluscan shellfish industry, and the critical aspect at this point is how to allow the industry to grow and prosper with such a threat. The industry cannot prevent outbreaks of harmful algal blooms that produce biotoxins and must therefore find approaches to manage the issue. Thus, the development of new inexpensive and ecologically sustainable technologies remains a great challenge. One approach is the use of photocatalysis which is based on the generation of very reactive species that can oxidize a wide spectrum of organic matter.

It is well established that titanium dioxide (TiO_2) is the best candidate for photocatalytic applications: it is nontoxic, chemically stable, tunable due to size effects, etc. [9–11]. Under UV irradiation of photon energy greater than or equal to the TiO_2 band gap energy ($h\nu > 3.2$ eV, i.e. $\lambda < 380$ nm), electron–hole pairs are formed, which once dissociated, generate free photo electrons and holes that are able to interact with organic matter present at a TiO_2 particle surface. The O_2 molecule scavenges an electron from the conduction band of TiO_2 to form a superoxide radical (O_2^-) because the energy of the conduction band edge is close to the reduction potential of oxygen. This superoxide reacts with a proton and an hydroperoxyl radical is formed ($HO_2^\bullet$). These O_2^- and $HO_2^\bullet$ species interact with organic pollutants and degrade them to CO_2, which is a harmless product [12]. Thus, through a complex multi-step heterogeneous photocatalytic process, an oxidative decomposition of organic molecules can be induced.

Since pioneering work performed in the early 1990s [9], the sol–gel processing of TiO_2 photocatalysts has been the subject of a continuously growing interest in several application fields. In particular, it has been reported in many articles that the sol–gel process is a versatile method for the preparation of optical quality photocatalytic TiO_2 thin films. For instance, these films have been studied for indoor atmosphere improvement, because odour-causing organic matter can be decomposed through a photocatalytic process [13,14]. These films have also been proposed for the removal of aqueous pollutants, i.e. for water purification [15]. In the last decade, nanocrystalline titania films have attracted the attention due to their better overall performance over the traditional coarse-grained films [16]. Many recent studies report on improved photocatalytic properties of sol–gel nanocrystalline TiO_2 films deposited on glass or silica [17–19]. However, photocatalytic activities of such films are limited by the fact that efficient photo-induced charges (electrons and holes) are only generated in films composed of a well crystallized phase, and preferably in the anatase allotropic form [11]. Usually, the crystallization of amorphous sol–gel TiO_2 films requires a post-deposition thermal treatment at relatively high temperatures (300 °C or above). Mostly, the TiO_2 films are coated on the surface of common soda-lime (SL) glass. However, it is known that the diffusion of Na^+ ions into the nascent TiO_2 film from the SL glass substrates during the heat-treatment process significantly deteriorates the photocatalytic activity [14,20–22]. To prevent the negative effect of sodium ions on photocatalytic activity, many methods, such as precoating SL glass with a SiO_2 layer or soaking the glass in a HNO_3 solution to exchange sodium ions, have been reported [21–23]. In this respect, a process to prepare nanocrystalline anatase TiO_2 films at low temperature becomes of great interest [24,25]. This process is not only significant from the point of view of energy saving, but also because it offers the possibility to deposit thin films on common SL glass and on low thermal-resistant materials such as plastics or polymer sheets.

In this paper, for the first time, we report on the photocatalytic degradation of DA using nanocrystalline anatase TiO_2 films coated on SL glass substrates. These films, prepared via a sol–gel dip-coating method in the presence of PEG of different molecular weights (200, 400 and 600) were crystallized at a low temperature of 90 °C. Studies of the photocatalytic degradation of DA were also performed with films coated on fused quartz substrates, crystallized at low temperature and subsequently annealed at 500 and 900 °C. The TiO_2 films were characterized for their microstructural and optical properties. Photocatalytic activity was quantified as the rate of disappearance of DA, as analyzed by HPLC.

2. Experimental methods

2.1. TiO_2 film preparation

As described elsewhere [25], for the preparation of the PEG-containing TiO_2 films, titanium tetra-*n*-butoxide (TTB) was used as the starting material. TTB was first mixed with a small amount of ethanol (EtOH) after which a mixture of water, HCl and EtOH was poured while stirring into the transparent solution to promote hydrolysis. Finally, an organic polymer (PEG) was added slowly to this mixture, and the resulting solution was used for the TiO_2 film coating. The sol–gel solutions were prepared in the presence of PEG of different molecular weights (200, 400 and 600); the molar ratio of PEG to TTB was one.

TiO_2 thin films were deposited onto SL glass and quartz substrates by dipping: the substrate was lowered into the coating solution and then withdrawn at a regulated speed of 4 mm/s. In some cases, the thickness of the films was increased by a second dipping. After each coating, the films were crystallized by a hot water treatment at a temperature of 90 °C for 1 h. Thereafter, some films were annealed at two different temperatures (500 or 900 °C). These samples were held at the specific temperature for 1 h and then cooled to room temperature. For the FTIR measurements, films deposited on silicon wafers under the same conditions were used.

2.2. TiO_2 film characterization

Raman spectra were recorded at room temperature with a Jobin-Yvon Labram HR microanalytical spectrometer equipped with a motorized *xy* stage and autofocus. The spectra were generated with a 17 mW, 632.8 nm He–Ne laser excitation and were dispersed with the 1800 g/mm grating across the 0.8 m length of the spectrograph. The laser power was 9 mW on the sample surface. The spectral resolution of this apparatus is estimated to be less than 0.5 cm^{-1} for a slit width of 150 μm and a confocal hole of 300 μm.

The infrared spectra of the dip-coated TiO_2 samples on silicon wafers were recorded with a Mattson FTIR spectrometer in a range of 400–4000 cm^{-1}.

X-ray diffraction measurements were carried out with a custom-built diffractometer equipped with graphite monochromator and analyzer crystals. Crystal sizes were determined based on the anatase (1 0 1) and (2 0 0) peaks using the Scherrer formula [26].

The optical constants and thickness of the films were obtained from a reflection/transmission spectroscopic ellipsometer.

For the band gap measurements, the transmission spectra of the films were recorded at normal incidence with a Biochrom Ultrospec 2000 UV-Visible spectrophotometer.

Scanning electron microscope (SEM) images were recorded for the films before hot water treatment at 90 °C, and for those crystallized at 90 °C, using a JEOL JSM-5600 SEM (JEOL USA, Peabody, MA). The microscope was operated at 10 kV, 10–15 mm working distance, and 45° specimen tilt.

2.3. Photocatalytic experiments

Domoic acid powder was purchased from Diagnostic Chemicals Limited (Prince Edward Island, Canada) and used as received. A stock solution of 28 000 ng DA/mL was prepared by dissolving DA in deionized water. The DA solution of 2500 ng DA/mL concentration, used in the photocatalytic experiments, was prepared by diluting the stock solution.

Irradiation was performed using a Luzchem irradiation chamber of ~32 cm (*W*) × 33 cm (*D*) × 21 cm (*H*), equipped with six top, four left side and four right side UVA lamps.

The photocatalytic experiments were performed in a cylindrical quartz cell having a 100 mL capacity. In a typical experiment, the cell was loaded with 80 mL of aqueous DA solution (2500 ng DA/mL), and then a TiO_2 film coated on a SL glass or quartz substrate was immersed in it. The cell was then introduced into the Luzchem irradiation chamber and exposed to UVA (λ ~ 350 nm). The temperature of the chamber was about 3 °C above room temperature. The choice of UVA irradiation was made with the perspective of developing a safe device to be used for the degradation of DA by the molluscan shellfish industry.

After starting the photocatalytic reaction, small aliquots were periodically withdrawn from the reactor in order to measure the concentration of DA as a function of time. DA analysis was carried out by high performance liquid chromatography (HPLC) using a "Waters 486" chromatograph equipped with a Phenomenex Luna C-18(2) column (150 mm × 4.9 mm i.d., particle size of 5 μm). The composition of the mobile phase was 2 mL of H_3PO_4 (8.5%), 125 mL CH_3CN and 873 mL of deionized water. The flow rate was 1 mL/min. The HPLC analysis was carried out at 242 nm, the maximum of absorption by DA. The photocatalytic activity was quantified as the rate of disappearance of DA.

3. Results and discussion

3.1. Raman and XRD studies

Fig. 1 shows the Raman spectra of films obtained from a TiO_2 solution prepared in presence of PEG 600. The spectra show that a film is amorphous before the hot water treatment at 90 °C, whereas it is crystallized afterwards as evidenced by the presence of the characteristic anatase Raman modes at ~150, 404, 518 and 637 cm^{-1}. Also, only the typical features of anatase are present in the film annealed at 500 °C. At 900 °C, a mixed anatase–rutile phase is seen, which is evident from the humps at 448 and 608 cm^{-1}. The Raman spectra of the films obtained from the coating solutions prepared with PEG having a molecular weight of 200 and 400 look similar to the ones shown in Fig. 1. For all the TiO_2 samples (see Table 1) containing PEG and treated in hot water (90 °C), the main anatase Raman band is very broadened (up to ~32 cm^{-1}) and high-frequency shifted (up to ~151 cm^{-1}), displaying the main aspect of nanocrys-

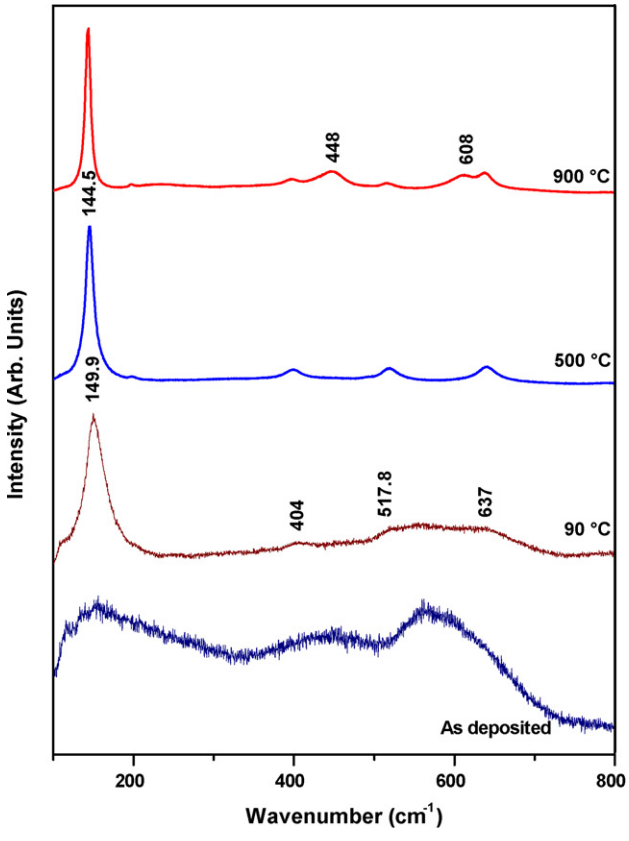

Fig. 1. Raman spectra of TiO_2 films prepared with PEG 600 and treated at different temperatures.

Table 1
Crystallite sizes of the TiO_2 anatase thin films prepared using PEG of molecular weight 200, 400 and 600 at various temperatures

Sample		Crystallite sizes from Raman data				Crystallite sizes from XRD measurements	
Molecular weight of PEG	Treatment temperature (°C)	Peak position (cm^{-1})	Size (nm)	FWHM (cm^{-1})	Size (nm)	Crystallite size (nm)	Error (nm)
200	90	151.2	6.0	30.4	4.0	4.3	0.6
	500	147.4	8.6	18.9	7.0	7.8	1.0
	900	–[a]	–	–	–	20.0	1.7
400	90	151.1	6.0	31.7	4.0	4.6	0.9
	500	149.1	7.2	23.3	5.6	5.7	0.7
	900	–[a]	–	–	–	18.5	0.9
600	90	149.9	6.7	32.1	4.0	4.8	0.4
	500	144.5	14.5	13.5	10.0	10.4	1.0
	900	–[a]	–	–	–	18.6	0.9

The crystallite sizes are obtained from Raman and XRD measurements and compared.
[a] Corresponds to a mixed anatase and rutile phase.

talline TiO_2 [25], when compared to the Raman spectrum of commercial anatase TiO_2 powder (Aldrich), which has the peak position (PP) at 142.5 cm^{-1} and a full width at half maximum (FWHM) of 7.5 cm^{-1}.

Using a phonon confinement model [27], it is possible to obtain an estimate of the crystallite size from the FWHM and the position of the anatase main Raman peak. The evolution of crystallite size is shown in Table 1. In the samples prepared with PEG 200, 400 and 600 and immersed in hot water for 1 h, the anatase main Raman peak is centered, respectively, at 151.2, 151.1 and 149.9 cm^{-1}, with a FWHM of 30.4, 31.7 and 32.1 cm^{-1}; each of these preparations gives a crystal size of ~5 nm. We attributed such large shifts and broadening of the main Raman band of the anatase phase mainly to the particle quantum size effect [27]. We can see that the crystallite size is independent of the molecular weight of the PEG used in the preparation of the samples. With the increase in the annealing temperature, the frequency and the width of the peaks tend towards those of the commercial anatase TiO_2 powder. Upon annealing the films at 500 °C, crystallite size increases to ~6, 7 and 10 nm for the samples prepared with PEG 400, 200 and 600, respectively.

Fig. 2 shows the XRD data of the TiO_2 film prepared in presence of PEG 200, 400 and 600. The samples evolve in identical ways upon heating. The as-deposited films are amorphous and scatter X-rays below 5 nm^{-1}, as well as between 11 and 18 nm^{-1}. Treatment in water eliminates most of the diffuse scattering, and leads to nanoscale anatase crystals. Annealing after treatment in hot water leads to a sharper anatase (1 0 1) peak at 17.85 nm^{-1}. The anatase (2 0 0) peak at 33.21 nm^{-1} is the second prominent peak of this phase. After treatment in hot water at 90 °C, the crystallite size is ~5 nm for samples prepared with PEG 200, 400 and 600. Upon annealing at 500 °C, the crystallite size increases to ~6, 8 and 10 nm for the films prepared with PEG 400, 200 and 600, respectively. For all the samples, the crystallite size increases to ~19 nm as the annealing temperature is raised to 900 °C, accompanied by a partial transformation to rutile. The XRD data are in good agreement with the Raman results discussed above.

3.2. FTIR studies

Fig. 3a shows the FTIR spectrum of the TiO_2 film containing PEG 600 deposited on a SL glass substrate before hot water treatment. The O–H stretching band is at 3457 cm^{-1}. The bands

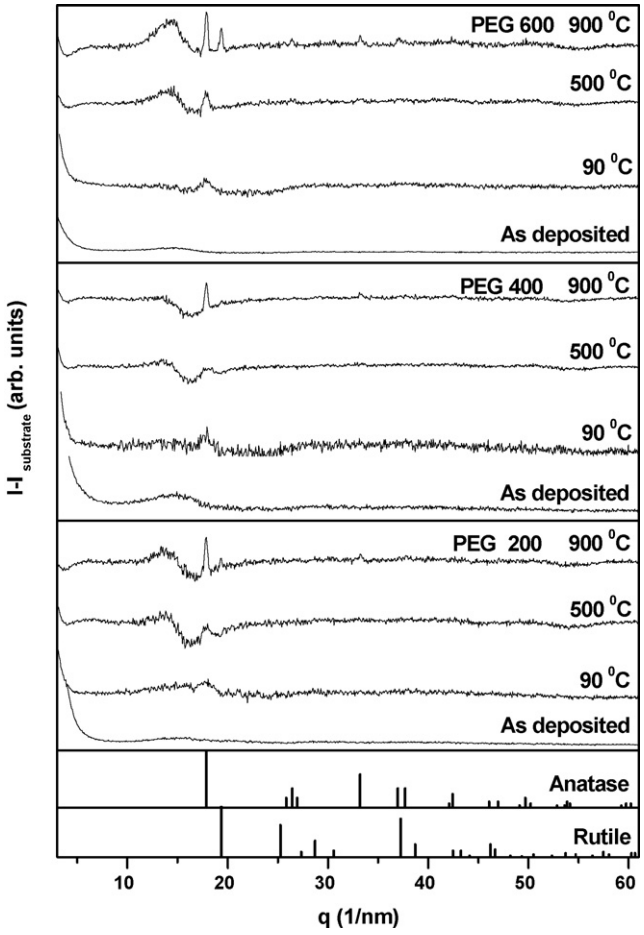

Fig. 2. XRD patterns of TiO_2 films prepared in presence of PEG 200, 400 and 600 as a function of heat treatment. The reference patterns of anatase and rutile are also shown for the purpose of comparison.

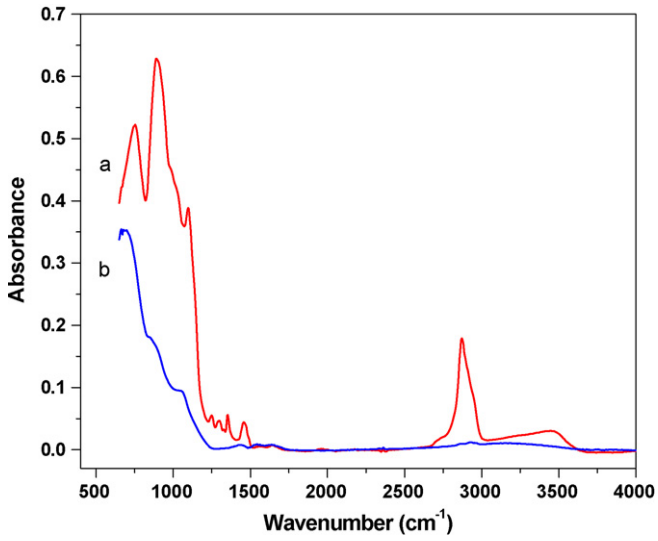

Fig. 3. FTIR spectra of TiO_2 films prepared with PEG 600: (a) before hot water treatment and (b) after hot water treatment at 90 °C for 1 h.

at 2862, 1462 and 1347 cm^{-1} correspond to the C–H vibrations, while the band centered at 1246 cm^{-1} originates from the C–O–C bonds of PEG. Fig. 3b shows the spectral changes occurring in the film after hot water treatment at 90 °C for 1 h. The bands corresponding to PEG disappear with the hot water treatment, indicating that the PEG molecules have been leached out of the film. Comparatively, Matsuda [24] showed that during a heat treatment in air, PEG starts to decompose only at ~250 °C and that a temperature of at least 300 °C is necessary to remove it completely from the film.

Fig. 4a shows the FTIR spectrum of a film containing PEG 600, indicating that the hydroxyl content after hot water treatment is high. This can be ascribed to the fact that some adsorbed H_2O can react with TiO_2 and form TiOH, such as, $H_2O + Ti{-}O{-}Ti \rightarrow 2TiOH$ [22]. However, the hydroxyl content decreased after the film was annealed at 500 °C (Fig. 4b) and was completely removed after annealing at 900 °C (Fig. 4c). In general, the presence of hydroxyl content on the surface of TiO_2 films is beneficial to the enhancement of photocatalytic activity [12].

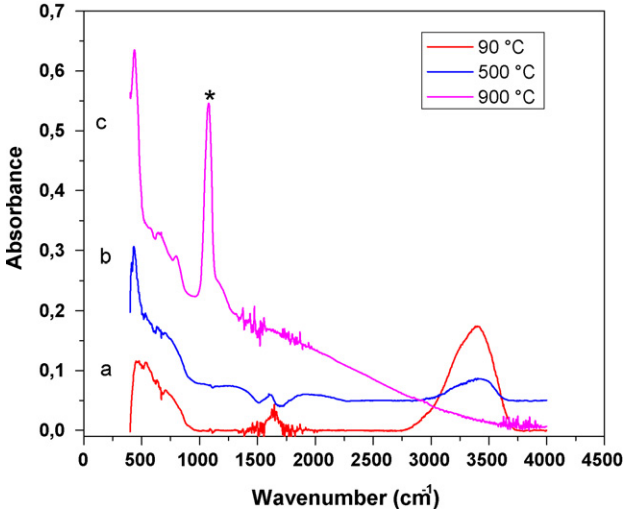

Fig. 4. FTIR spectra of TiO_2 films prepared with PEG 600 and treated at 90, 500 and 900 °C. The peak marked with an asterisk in (c) corresponds to the ν_{Si-O} vibration.

3.3. SEM studies

Fig. 5 shows SEM images of the films prepared from solutions having PEG of molecular weights 200, 400 and 600. The images on the left and right panel show the microstructure of the films before and after hot water treatment for 1 h, respectively. The cross-section of the film before hot water treatment is smooth and has high thickness. After hot water treatment, the cross-section of the film is rough, due to the formation of anatase nanocrystals, not only on the surface but also inside the film. The thickness of the film is also smaller than before hot water treatment, attributed to the removal of PEG. The removal of PEG has also resulted in a porous structure.

3.4. Optical properties

The refractive index and thickness of the films were obtained from spectroscopic ellipsometry measurements. These are presented in Table 2 for TiO_2 films prepared with PEG 200, 400 and 600 and treated at 90 °C. The refractive index at 632.8 nm is low for all the samples prepared with PEG (between 1.61 and 1.63), in comparison to the bulk value of 2.52 [28]. The observed reduction in the refractive index is attributed to the porosity of the films which varies from 62 to 71%. The porosity values (P), as presented in Table 2, were calculated from the refractive index measurements using the following equation:

$$P = 1 - \frac{n^2 - 1}{n_b^2 - 1} \quad (1)$$

where n_b and n are the refractive indices of bulk anatase and of the porous film, respectively [29].

Film porosity is an important factor that can influence photoactivity. Liquid or solid reactants are able to diffuse through the pores when they come into contact with the film surface, thus inducing a greater quantity of TiO_2 particles to be involved in the photocatalytic reaction.

As shown in Table 2, the thickness of the films increases from 200 to 306 nm for one layer, and from 413 to 668 nm for two layers, when the molecular weight of the PEG added to the coating solution is increased from 200 to 600. This is mainly due to an increase in the viscosity of the dipping solution as the molecular weight of the PEG is increased.

As the annealing temperature of a TiO_2 film is increased, the refractive index approaches the bulk value of 2.52 and the film porosity and thickness decrease. For example, the refractive index of the TiO_2 film obtained from a coating solution containing PEG 600 and heat treated at 500 °C was found to be 2.43 with a porosity of 8% and a thickness of 190 nm.

3.5. Optical band gap

In the high absorption region, near the absorption edge, the absorbance of a thin dielectric film is known to obey the relation:

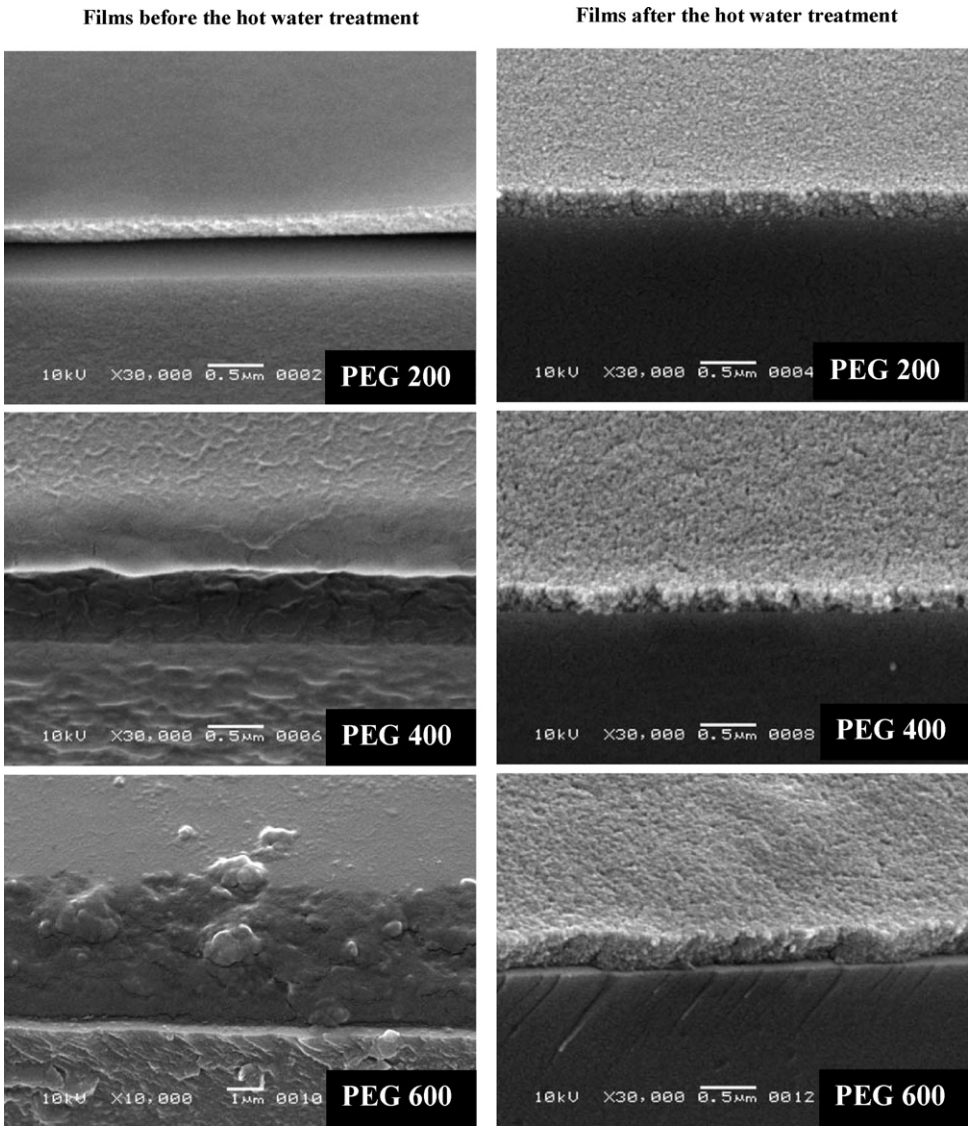

Fig. 5. Microstructure of the TiO_2 films before and after hot water treatment, as observed by scanning electron microscopy.

$$\alpha h\nu = A(h\nu - E_g)^n, \quad (2)$$

where α is the absorption coefficient, A is a constant and E_g is the optical band gap of the film [30]. For the anatase polymorph of TiO_2, the optical transition is indirect, and $n=2$ in Eq. (2). Furthermore, in the region of strong absorption, and at normal incidence, the reflectivity is very small and can be neglected [31]. This leads to the following expression for the absorption coefficient α as a function of transmittance T:

$$\alpha = -2.303\frac{\log T}{t}, \quad (3)$$

where t is the film thickness [31]. Eq. (2) then becomes $-2.303\ h\nu \log T = B(h\nu - E_g)^2$, and the graph of $(-2.303\ h\nu \log T)^{1/2}$ versus $h\nu$ will present a linear part that can be extrapolated to zero, leading to E_g.

Table 2
Optical properties and thicknesses of TiO_2 anatase thin films prepared using PEG of molecular weights 200, 400 and 600 and treated at 90 °C

Sample prepared in presence of		Refractive index at 632.8 nm	Calculated porosity	Optical band gap (eV)	Thickness (nm)
PEG 200	One layer	1.61	0.70	3.55	200
	Two layers	1.63	0.69	3.51	413
PEG 400	One layer	1.63	0.69	3.54	247
	Two layers	1.59	0.71	3.51	518
PEG 600	One layer	1.63	0.68	3.54	306
	Two layers	1.73	0.62	3.25	668

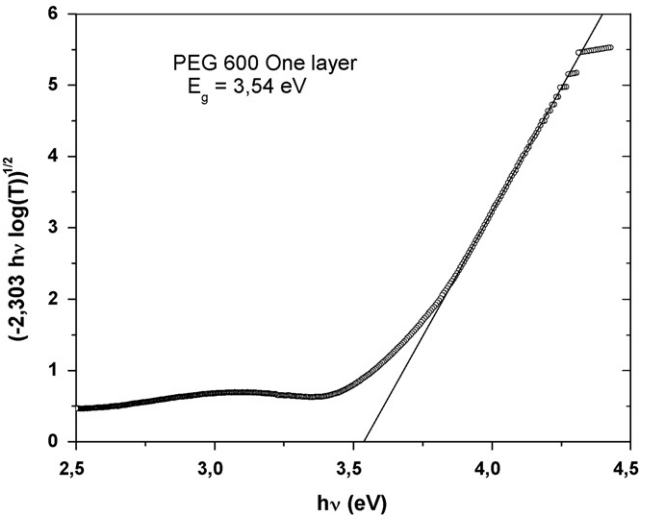

Fig. 6. Optical band gap of a TiO_2 thin film.

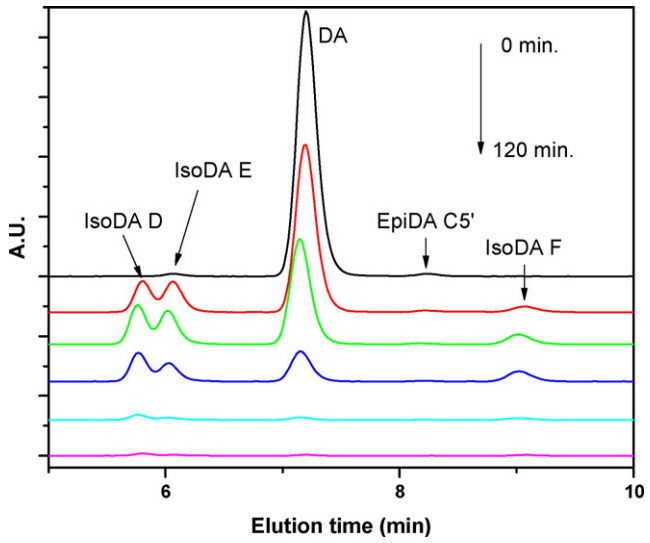

Fig. 7. Chromatograms showing changes in the concentration of domoic acid (DA) and its isomers during photodegradation.

The transmittance variation of the TiO_2 thin films near the absorption edge was analysed according to the above-described procedure. Fig. 6 shows an example of the $(-2.303\ h\nu \log T)^{1/2}$ versus $h\nu$ graph for a film prepared with PEG 600.

As presented in Table 2, the band gap of the TiO_2 films prepared with PEG of molecular weights 200, 400 and 600, after hot water treatment (90 °C), is ∼3.55 eV. This is greater than the 3.20 eV band gap value of bulk anatase TiO_2 [32], and is attributed to the nanocrystalline sizes of the TiO_2 crystallites.

3.6. Nanocrystalline TiO_2 thin film assisted photodegradation of domoic acid

The photocatalytic activity of films deposited on SL glass and fused quartz substrates was studied by DA photodecomposition tests. In this work, a UV irradiation of ∼350 nm (UVA) was used. DA analysis was done by HPLC, and the photocatalytic activity was quantified as the rate of disappearance of DA.

DA is a tricarboxylic amino acid related structurally to glutamic acid. Its molecular structure can be seen in Scheme 1. It possesses a side chain containing a conjugated double bond moiety and a hind carboxylic acid. The double bonds at C-1′ and C-3′ are *Z* and *E* isomers, with an R-configuration at C-5′ center denoting this toxin as 1′-*Z*,3′-*E*,5′-R(−)-domoic acid. The geometry of the double bonds in the side chain is related to the potency of the toxin.

Fig. 7 shows typical time-dependent HPLC-UV chromatograms obtained during the TiO_2-mediated photocatalytic

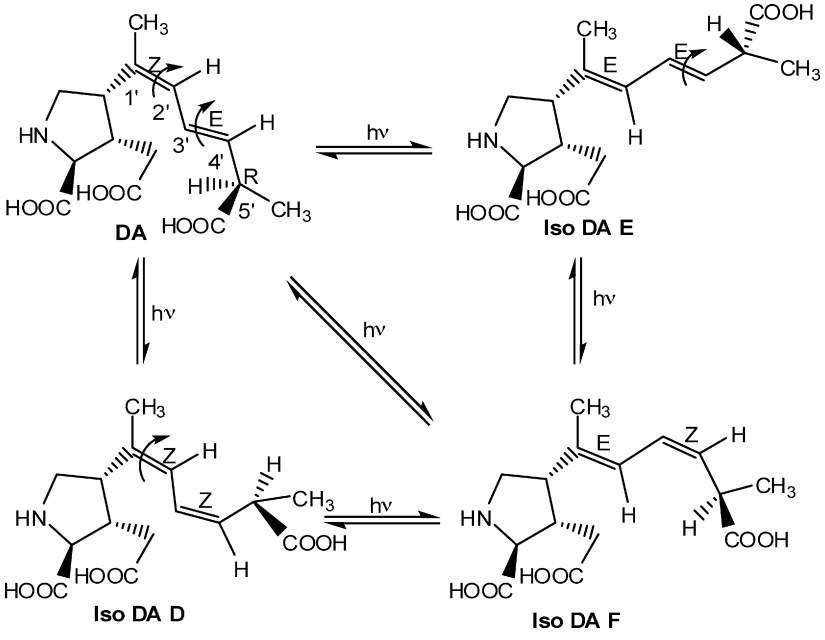

Scheme 1.

degradation of aqueous solution of DA under UV irradiation. The chromatogram obtained prior to immersing the photocatalyst (top trace) shows three peaks: the main DA peak and two other peaks corresponding to IsoDA E, and EpiDA C5′. However, the contribution of IsoDA E (0.5%), and EpiDA C5′ (0.8%) is negligible, compared to that of DA (98.7%). From this chromatogram, it is also seen that IsoDA E is eluted first, followed by the main peak attributed to DA. The last peak identified in this chromatogram belongs to EpiDA C5′.

3.7. Degradation of domoic acid without photocatalyst

Fig. 8 shows the profiles of the time-dependant degradation of DA after exposure to daylight (star trace), and to a UV irradiation of ∼350 nm (triangle trace), without photocatalyst. No significant degradation of DA was seen after exposure to daylight alone, and exposure to UVA light for 4 h resulted in a negligible DA degradation (<8%).

3.8. Factors influencing the effectiveness of the TiO_2 photocatalyst

3.8.1. Influence of substrate

The composition and properties of fused quartz and glass are different. SL glass contains a large amount of sodium ions (about 10–15 wt% Na_2O) and possesses a lower thermal stability. When TiO_2 films deposited on SL glass substrates are annealed at a high temperature, a lot of sodium ions diffuse from the glass into the nascent TiO_2 films [12,14,21,23]. According to Paz and Heller [20], a high concentration of sodium could prevent the formation of the photoactive anatase phase, and a low concentration of sodium could produce surface and bulk recombination centers of photo-generated electron–hole pairs. In this work, we overcome the deleterious effect of sodium by crystallizing the TiO_2 films deposited on SL glass at a low temperature of 90 °C, and by using fused quartz substrates for films annealed at higher temperatures (500 and 900 °C).

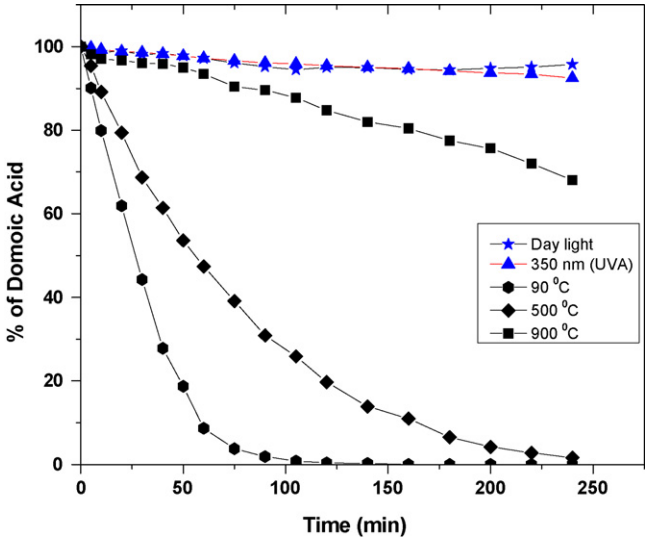

Fig. 8. Degradation profiles of domoic acid with time, when exposed to daylight and UVA (∼350 nm) without photocatalyst, and when exposed to UVA light with TiO_2 films prepared with PEG 600 and heat treated at different temperatures.

3.8.2. Influence of heat treatment of the films

Fig. 8 also shows the degradation of DA in aqueous solution when exposed to UVA light in the presence of three types of TiO_2 films prepared from a coating solution containing PEG 600. It can be seen that the TiO_2 film deposited on a SL glass substrate, and crystallized at 90 °C for 1 h in hot water, exhibited a better photocatalytic activity than the films deposited on a fused quartz substrate, crystallized at 90 °C for 1 h in hot water and subsequently annealed at 500 or 900 °C for 1 h.

For the TiO_2 film annealed at 900 °C, a decrease of 30% in DA concentration (relative to the time zero value) is observed after exposure to UVA light for 4 h. For the TiO_2 film annealed at 500 °C, the photodegradation was faster, as only 3% DA remained after the same time exposure. For the TiO_2 film crystallized by hot water at 90 °C, and with no further annealing, the decrease was more dramatic; no detectable DA remained after 2 h and 40 min of exposure to UVA light.

The TiO_2 film prepared with PEG 600 and treated in water at 90 °C leads to nanoscale anatase crystallites of ∼5 nm (see Table 1). The degradation of DA with this film was very fast. It is known that the photocatalytic activity of TiO_2 films is limited by the fact that efficient photo-induced charges (electrons and holes) are only generated in well-crystallized phases, and preferably in the anatase allotropic form [11]. Apart from the degree of crystallization that determines the photo-induced charge carrier generation in TiO_2 grains, the small crystallite size is another factor that advantageously influences the photocatalytic activity of the film [33]. First, it can provide a greater contact surface exposed to the DA to be decomposed. Second, it reduces the probability of bulk electron–hole pair recombination, which is known to severely limit the efficiency of photocatalytic reactions [34].

The film that was heated at 500 °C is also found to have anatase crystallites, but with an increased grain size (∼10 nm). Although the degradation of DA with this film was complete, it was relatively slow when compared to the film crystallized at 90 °C. We attribute this slower degradation to the increase in crystallite size which diminishes the contact surface area. The film annealed at 900 °C shows very low photocatalytic activity when compared to the films treated at 90 or 500 °C. Here, DA is degraded only by 30% after 4 h. As mentioned earlier, this film had a mixed phase of both rutile and anatase, with a crystallite size of ∼20 nm. Although Bickley et al. [35] suggested that the anatase/rutile structure has high photoreactivity owing to the slow charge recombination, there are many reports claiming rutile is either much less active [36–39] or catalytically inactive [40–42]. For example, Kato et al. [43] used a mixed phase thin film of anatase and rutile for the photodegradation of aqueous acetic acid and found that the photoactivity was increased as the anatase fraction in the film was increased. In our case, the degradation of DA was reduced by the presence of the rutile crystallites in the film.

Also, according to Kato et al. [43], an increase in the surface hydroxyl content traps more photo-generated holes and

prevents electron–hole recombination, thus enhancing the photocatalytic activity. The FTIR spectra in Fig. 4, showing a decreasing amount of hydroxyl group content with increasing treatment temperature of the films, and the photodegradation results reported in Fig. 8, showing a decrease in the photodegradation efficiency with increasing treatment temperature of the films, are in accordance with the observations of Kato et al.

Since the photocatalytic reaction is enhanced by the possibility of DA to diffuse through pores in the film, the film porosity is also an important factor influencing the photodegradation process. Due to densification, the film annealed at a high temperature presents less porosity than the films prepared at a lower temperature. Thus, the difference in the photocatalytic activity of the films could be due to a change in porosity as well as to a difference in the crystallite size and hydroxyl group content at the surface.

3.8.3. *Influence of PEG*

In order to understand the nature of the influence of PEG on DA photodegradation, TiO_2 films were coated on SL glass substrates from sol–gel solutions that were prepared in the presence of PEG of different molecular weights (200, 400 and 600). Those films, crystallized at 90 °C, exhibited a porosity of ∼70%, and a crystallite size of ∼5 nm. Thus, porosity and crystallite size do not explain the differences observed in the photodegradation results from Fig. 9, where it can be seen that the DA degradation increases with the increasing molecular weight of the PEG used in the sample preparation. Complete degradation occurs after 4.5 h in the case of the films prepared with PEG 200, whereas for the films prepared with PEG 600, the degradation time is reduced to 2 h and 40 min. Again, the FTIR results presented in Fig. 10 show that the TiO_2 film prepared in presence of PEG 600 and crystallized at low temperature contains more hydroxyl groups than that of the film prepared with PEG 400, which in turn contains more hydroxyl groups than that of the film prepared with PEG 200, explaining in part the photodegradation results from Fig. 9.

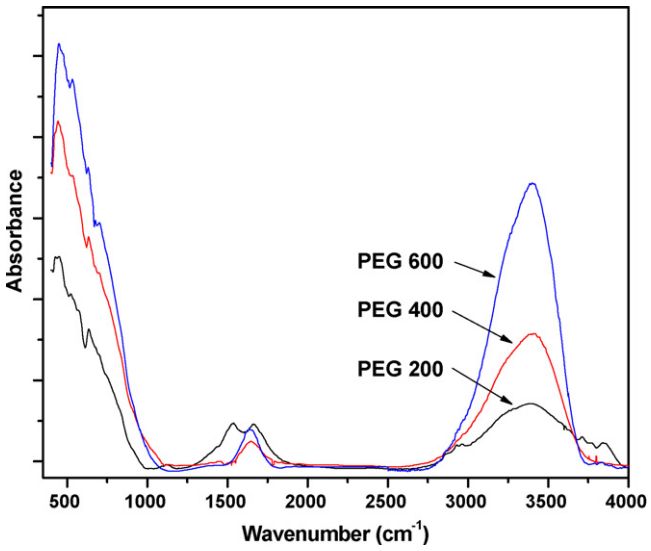

Fig. 10. FTIR spectra of the TiO_2 samples prepared with PEG 200, 400 and 600, after hot water treatment at 90 °C.

Apart from porosity, crystallite size, and the hydroxyl group content at the surface, the film thickness could play an important role in the photodegradation of DA by porous thin films. Fig. 11 shows the photocatalytic activity of TiO_2 films prepared with PEG 200 and deposited by one and two dippings, having a thickness of 200 and 413 nm, respectively. The films were deposited on SL glass substrates and crystallized at 90 °C in hot water. The complete degradation of DA occurs after 4.5 h in the case of the film obtained after one dipping (200 nm), while for the film prepared by two dippings (413 nm), the degradation time is reduced to 3.5 h. This supports the finding that stronger catalytic activity can be achieved with thicker films.

Table 2 indicates that, as the molecular weight of PEG used in the sample preparation is increased from 200 to 600, the thickness of the films also increases from 200 to 306 nm, because the viscosity of the dipping solution increases accordingly. Hence, in addition to porosity, crystallite size, and hydroxyl group content,

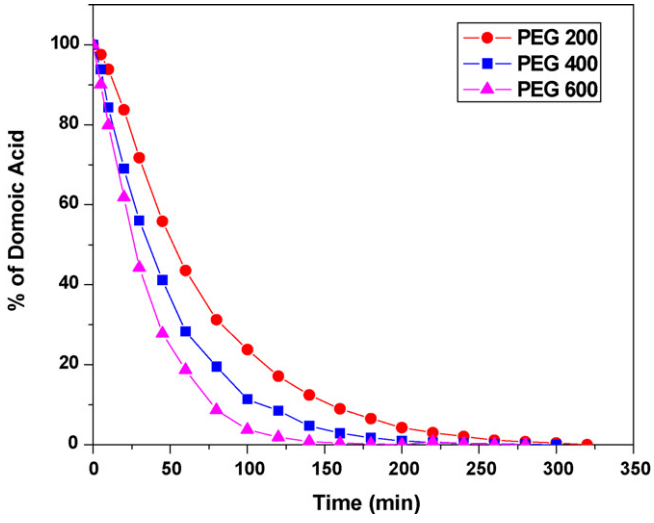

Fig. 9. Degradation profiles of domoic acid with time, using TiO_2 films prepared with PEG 200, 400 and 600, and crystallized at low temperature (90 °C).

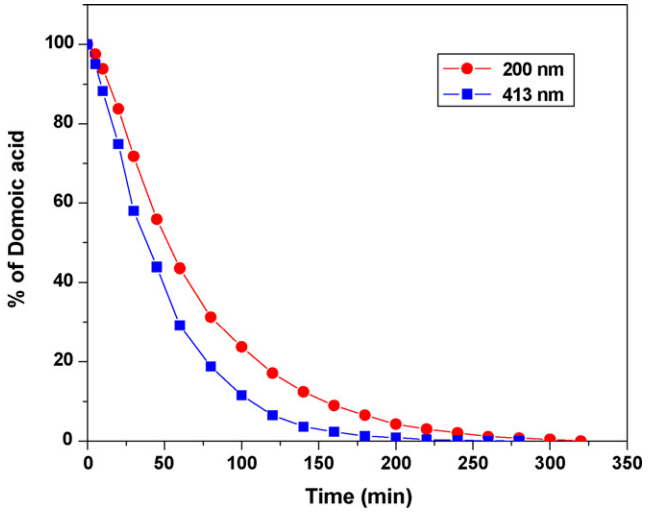

Fig. 11. Degradation profile of domoic acid using the TiO_2 films prepared with PEG 200 and having thickness of 200 and 413 nm.

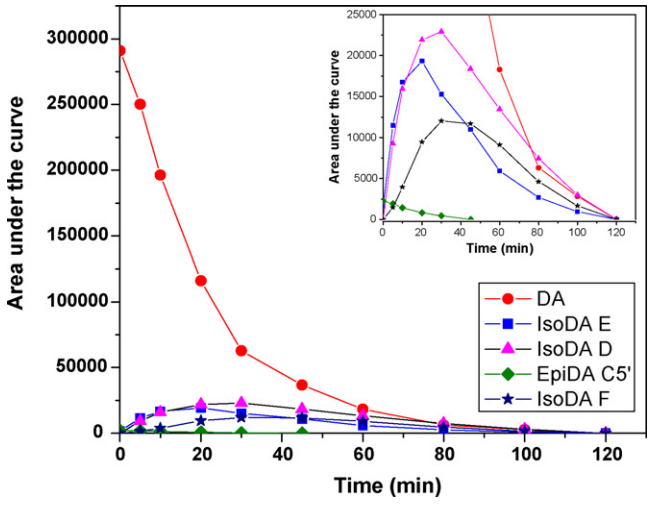

Fig. 12. Amounts of domoic acid (DA) and its isomers obtained as a function of time during photodegradation. Inset shows the enlarged region, displaying better the initial amounts and its evolution with time.

thickness is also a factor influencing the photocatalytic activity of these thin films. It can also be observed that the film obtained from a solution prepared using PEG 200 and having a thickness of 413 nm (see Fig. 11) is a less efficient photocatalyst than the film obtained from a solution prepared using PEG 600 having a lesser thickness of 306 nm (PEG 600 in Fig. 9). This observation tend to indicate that the hydroxyl group content at the surface of the film plays a more important role than thickness in the photodegradation of DA.

3.8.4. Mechanism of domoic acid photodegradation

During photodegradation, the presence, transformation and degradation of various DA isomers were observed, as seen in Fig. 7, which shows the typical evolution of the HPLC chromatograms as a function of photodegradation elapsed time. After immersing a TiO_2 film in the DA solution, and following UV light illumination, the peaks corresponding to DA and its isomers decrease with time and eventually disappear, indicating that DA has been degraded.

Fig. 12, which was extracted from similar chromatograms, shows the degradation of DA by UVA radiation and the TiO_2 photocatalyst prepared with PEG 600 as a function of time. In this case, the thickness of the TiO_2 film is 668 nm. The DA starting solution consists of 98.7% DA, 0.5% IsoDA E, and 0.8% EpiDA C5′. After 5 min of degradation, the concentration of DA was reduced by 14%, from 98.7 to 84.8%. Of these 14%, 7% was completely degraded and the other 7% was transformed into DA isomers. Besides IsoDA E and EpiDA C5′, we observed the formation of two isomers that were not present in the starting solution, i.e. IsoDA F (0.5%) and IsoDA D (3.1%) (after 5 min exposure). The concentration of IsoDA E increased to 3.9%, whereas the concentration of the EpiDA C5′ isomer was reduced to 0.7% (after 5 min exposure). Thus, during DA degradation, a portion of DA was transformed into its isomers (i.e. IsoDA E, IsoDA D and IsoDA F). After reaching a maximum concentration (6.6% for IsoDA E after 20 min, and 7.8 and 4.1% for IsoDA D and IsoDA F, respectively, after 30 min), these isomers started to degrade. DA, including its isomers, was completely degraded in less than 2 h. These results are summarized in Table 3.

The formation of IsoDA D, IsoDA E and IsoDA F can be explained by isomerization of the alkene double bonds as shown in Scheme 1. When 1′-*Z*,3′-*E*,5′-*R*(−)-domoic acid undergoes one bond flipping (OBF) at the C1′=C2′ bond, 1′-*E*,3′-*E*-isodomoic acid (IsoDA E) is formed. Similarly, when OBF takes place at the C3′=C4′ bond of 1′-*Z*,3′-*E*,5′-*R*(−)-domoic acid, 1′-*Z*,3′-*Z*-isodomoic acid (IsoDA D) is formed. The formation of IsoDA F can be explained in several ways: by the OBF of IsoDA E at the C3′=C4′ bond, by the OBF of IsoDA D at the C1′=C2′ bond, or by two OBFs of DA at the C1′=C2′ bond and another at the C3′=C4′ bond, taking place simultaneously as shown in Scheme 1. Photoisomerization of dienes and trienes is reviewed by Liu and Hammond [44].

A possible mechanism of DA degradation is shown in Scheme 2. Zwitter-ionic DA undergoes cleavage at the pyrrolidine ring to give intermediate **A**. Intermediate **A** gives intermediate **B** with the expulsion of CO_2. There are two possibilities for intermediate **B** to form intermediate **D**, with hydroxyl radical abstraction: (i) formation of $–NHCH_2OH$ followed by the metathetical elimination of formaldehyde and ammonia, leading to the formation of aldehyde **C**; the oxidation of **C** under photochemical conditions by an O_2 radical gives intermediate **D**; (ii) formation of $–N^+H(OH)CH_3$, which abstracts an hydroxyl radical and forms intermediate **D**, with the expulsion of NO_3^- and CO_2. Hidaka et al. [45] proposed a similar mechanism for the degradation of amino acids, with the elimination of NO_3^-, NH_3 and CO_2.

Table 3
Degradation of domoic acid (DA) and subsequent evolution of its isomers at various time intervals during photocatalytic degradation of domoic acid (DA)

Sample	Time (min)	DA (%)	ISO E (%)	ISO D (%)	ISO C5′ (%)	ISO F (%)	Total (%)	Degraded (%)
1	0	98.7	0.5	0	0.8	0	100.0	0.0
2	5	84.8	3.9	3.1	0.7	0.5	93.0	7.0
3	10	66.5	5.7	5.4	0.5	1.3	79.4	20.6
4	20	39.3	6.6	7.4	0.3	3.2	56.8	43.2
5	30	21.3	5.2	7.8	0.1	4.1	38.5	61.5
6	45	12.4	3.7	6.2	0	4.0	26.4	73.6
7	60	6.2	2.0	4.6	0	3.1	15.8	84.2
8	80	2.1	0.9	2.5	0	1.6	7.1	92.9
9	100	1.0	0.3	1.0	0	0.6	2.9	97.1
10	120	0	0	0	0	0	0	100.0

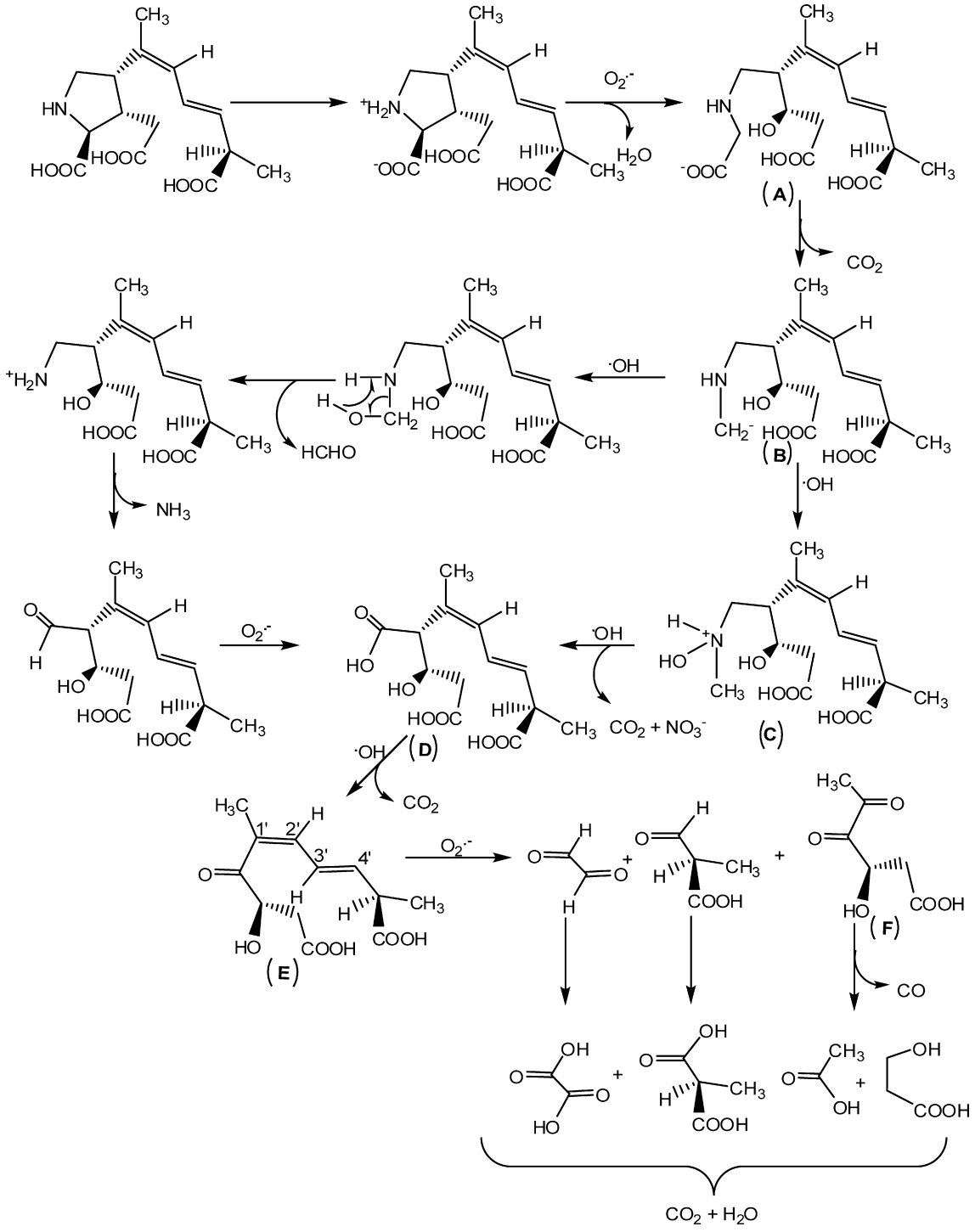

Scheme 2.

By the abstraction of an OH radical, intermediate **D** undergoes decarboxylation to form **E**. Intermediate **E** undergoes oxidative cleavage at C1′ = C2′ to give 2-oxo acetic acid, *R*-2-methyl-3-oxopropanoic acid, and oxidative cleavage of **E** at C3′ = C4′ leads to the formation of 3-hydroxy-4,5-dioxo hexanoic acid (**F**). Oxaladehyde is oxadized to oxalic acid, whereas *R*-2-methyl-3-oxopropanoic acid is oxidized to 2-methyl malonic acid. Intermediate **F** undergoes α-cleavage to form acetic acid and 3-hydroxy propanoic acid with the expulsion of CO. Finally, all of these products (oxalic acid, 2-methyl malonic acid, acetic acid and 3-hydroxy propanoic acid) are converted to CO_2 and water.

4. Conclusion

Porous nanocrystalline anatase TiO_2 thin film photocatalysts were successfully prepared by using PEG as a structure-directing agent and a hot water treatment of 90 °C. Films were also pre-

pared using a high temperature treatment of 500 and 900 °C. Raman and XRD studies revealed the nanocrystalline nature of the films prepared at 90 and 500 °C, and a mixed phase formation of anatase and rutile in the films that were heat treated at 900 °C. FTIR measurements indicated the presence of hydroxyl ions on the films surface, while confirming the absence of organic materials in the films that were treated in hot water for 1 h. The hydroxyl ions were absent from the surface of the films treated at 900 °C, while they appeared in a decreasing amount on the surface of the films prepared in presence of PEG 600, 400 and 200. Optical studies revealed a porosity of ∼70%. The films have large band gap attributed to the size of the crystallite particles. Photodegradation of DA, carried out under UVA irradiation, indicated that the degradation was effective only in the presence of the TiO_2 photocatalyst. Further, the photodegradation was found to be strongly dependent on the crystalline nature and crystallite sizes of the films. The films prepared at 500 °C showed less activity than those prepared by hot water treatment alone. The mixed phase thin films having both rutile and anatase were not effective photocatalysts for DA. The photodegradation rate depended on the thickness of the films, and both the rate and the thickness increased with the molecular weight of the PEG used in the coating solution. During photodegradation, this heterogeneous catalytic process leads to the partial transformation of DA to its isomers, and finally to its complete degradation. All the transformed isomers of DA, along with DA, are completely destroyed within 120 min irradiation using the TiO_2 film prepared with PEG 600. The mechanisms of the partial isomerization of DA and of the photodegradation of DA were presented. This TiO_2-assisted photodegradation of DA offers a broad scope of applications to the molluscan shellfish industry, especially during harmful algal blooms.

Acknowledgements

The financial support of the New Brunswick Innovation Fund (NBIF), the Research Assistantships Initiative (NBIF), the Consortium national de formation en santé (CNFS) volet Université de Moncton, concours 2006–2007, and of the Atlantic Innovation Fund (AIF) Round I, is gratefully acknowledged. We thank Dr. Sylvain Poirier (former director of the Centre de recherche sur les produits marins, Shippagan, NB, Canada) for providing the HPLC instrument, and James Ehrman (Digital Microscopy Facility, Mount Allison University, Sackville, NB, Canada) for the scanning electron micrographs.

References

[1] S.S. Bates, J. Phycol. 36 (2000) 978–983.
[2] S.S. Bates, D.L. Garrison, R.A. Horner, in: D.M. Anderson, A.D. Cembella, G.M. Hallegraeff (Eds.), Physiological Ecology of Harmful Algal Blooms, Springer-Verlag, Heidelberg, 1998, pp. 267–292.
[3] J.L.C. Wright, R.K. Boyd, A.S.W. de Freitas, M. Falk, R.A. Foxall, W.D. Jamieson, M.V. Laycock, A.W. McCulloch, A.G. McInnes, P. Odense, V. Pathak, M.A. Quilliam, M.A. Ragan, P.G. Sim, P. Thibault, J.A. Walter, M. Gilgan, D.J.A. Richard, D. Dewar, Can. J. Chem. 67 (1989) 481–490.
[4] C.A. Scholin, F. Gulland, G.J. Doucette, S. Benson, M. Busman, F.P. Chavez, J. Cordaro, R. DeLong, A. De Vogelaere, J. Harvey, M. Haulena, K. Lefebvre, T. Lipscomb, S. Loscutoff, L.J. Lowenstine, R.I. Martin, P.E. Miller, W.A. McLellan, P.D.R. Moeller, C.L. Powell, T. Rowles, P. Silvagnl, M. Silver, T. Spraker, V. Trainer, F.M. Van Dolah, Nature 403 (2000) 80–84.
[5] K.A. Lefebvre, S. Bargu, T.K. Ieckhefer, M.W. Silver, Toxicon 40 (2002) 971–977.
[6] J.E. Stewart, L.J. Marks, M.W. Gilgan, E. Pfeiffer, B.M. Zwicker, Can. J. Microbiol. 44 (1998) 456–464.
[7] S.S. Bates, C. Léger, M.L. Wells, K. Hardy, in: S.S. Bates (Ed.), Proceedings of the Eighth Canadian Workshop on Harmful Marine Algae. Can. Tech. Rep. Fish. Aquat. Sci. No. 2498, 2003, pp. 30–35.
[8] J.M. Fisher, J.G. Reese, P.J. Pellichia, P.L. Moeller, J.L. Ferry, Environ. Sci. Technol. 40 (2006) 2200–2205.
[9] S. Tunesi, M. Anderson, J. Phys. Chem. 95 (1991) 3399–3405.
[10] N. Serpone, E. Pelizetti (Eds.), Photocatalysis. Fundamentals and Applications, John Wiley & Sons, New York, 1989.
[11] J.M. Herrmann, Catal. Today 53 (1999) 115–129.
[12] M.R. Hoffmann, S.T. Martin, W. Choi, D.W. Bahnemann, Chem. Rev. 95 (1995) 69–96.
[13] V. Romeas, P. Pichat, C. Guillard, T. Chopin, C. Lehaut, Ind. Eng. Chem. Res. 38 (1999) 3878–3885.
[14] Y. Paz, Z. Luo, L. Rabenberg, A. Heller, J. Mater. Res. 10 (1995) 2842–2848.
[15] A. Fernandez, G. Lassaletta, V.M. Jimenez, A. Justo, A.R. Gonzalez-Elipe, J.M. Herrmann, H. Tahiri, Y. Ait-Ichou, Appl. Catal. B: Environ. 7 (1995) 49–63.
[16] G. Sberveglieri, L.E. Depero, M. Ferroni, V. Guidi, G. Martinelli, P. Nelli, C. Perego, L. Sangaletti, Adv. Mater. 8 (1996) 333–337.
[17] N. Negishi, K. Takeuchi, J. Sol–Gel Sci. Technol. 22 (2001) 23–31.
[18] A. Hattori, H. Tada, J. Sol–Gel Sci. Technol. 22 (2001) 47–52.
[19] N. Smirnova, A. Eremenko, O. Rusina, W. Hopp, L. Spanhel, J. Sol–Gel Sci. Technol. 22 (2001) 109–113.
[20] Y. Paz, A. Heller, J. Mater. Res. 12 (1997) 2759–2766.
[21] J. Yu, X. Zhao, Mater. Res. Bull. 35 (2000) 1293–1301.
[22] J. Yu, X. Zhao, Mater. Res. Bull. 36 (2001) 97–107.
[23] A. Fujishima, R.T. Narasinga, Proc. Indian Acad. Sci. Chem. Sci. 109 (1997) 471–486.
[24] A. Matsuda, Y. Kotani, T. Kogure, M. Tatsumisago, T. Minami, J. Am. Ceram. Soc. 83 (2000) 229–254.
[25] Y. Djaoued, S. Badilescu, P.V. Ashrit, D. Bersani, P.P. Lottici, R.J. Bruning, J. Sol–Gel Sci. Technol. 24 (2002) 247–254.
[26] E. Bertaud, International Tables for X-ray Crystallography, Kynoch Press, Birmingham, England, 1968, p. 318.
[27] S. Balaji, Y. Djaoued, J. Robichaud, J. Raman Spectrosc. 37 (2006) 1416–1422.
[28] W.D. Kingery, H.K. Bowen, D.R. Uhlmann, Introduction to Ceramics, Wiley, New York, 1976, pp. 647–703.
[29] B.E. Yoldas, Appl. Opt. 19/9 (1980) 1425–1429.
[30] J. Tauc, Optical Properties of Solids, Academic Press, New York, 1966, pp. 277–313.
[31] A.G. Vedeshwar, J. Phys. III France 5 (1995) 1161–1172.
[32] L. Kavan, M. Grätzel, S.E. Gilbert, C. Klemens, H.J. Scheel, J. Am. Chem. Soc. 118 (1996) 6716–6733.
[33] A.L. Linsebigler, G. Lu, J.T. Yates Jr., Chem. Rev. 95 (1995) 735–758.
[34] A. Hattori, Y. Tokihisa, H. Tada, N. Tohge, S. Ito, K. Hongo, R. Shiratsuchi, G. Nogami, J. Sol. Gel Sci. Technol. 22 (2001) 53–61.
[35] R.I. Bickley, T. Gonzalez-Carreno, J.S. Lees, L. Palmisano, R.J.D. Tilley, J. Solid State Chem. 92 (1991) 178–190.
[36] H. Noda, K. Oikawa, H. Kamada, Bull. Chem. Soc. Jpn. 66 (1995) 455–458.
[37] B. Ohtani, S. Nishimoto, J. Phys. Chem. 97 (1993) 920–926.
[38] B.V. Mihaylov, J.L. Hendrix, J.H.J. Nelson, Photochem. Photobiol. A: Chem. 72 (1993) 173–177.
[39] K.E. Karakitsou, X.E. Verykios, J. Phys. Chem. 97 (1993) 1184–1189.

[40] A. Mills, S. Morris, R.J. Davies, J. Photochem. Photobiol. A: Chem. 70 (1993) 183–191.
[41] A. Mills, R.H. Davies, D. Worsley, Chem. Soc. Rev. 22 (1993) 417–425.
[42] S.T. Martin, C.L. Morrison, M.R. Hoffmann, J. Phys. Chem. 98 (1994) 13695–13704.
[43] K. Kato, A. Tsuzuki, H. Taoda, Y. Torii, T. Kato, Y. Butsugan, J. Mater. Sci. 29 (1994) 5911–5915.
[44] R.S.H. Liu, G.S. Hammond, Photochem. Photobiol. Sci. 2 (2003) 835–844.
[45] H. Hidaka, S. Horikoshi, K. Ajisaka, J. Zhao, N. Serpone, J. Photochem. Photobiol. A: Chem. 108 (1997) 197–205.